Autonomous Robots manuscript No.
(will be inserted by the editor)

Design of a Partially-Coupled Self-Adaptive Robotic Finger Optimized for Collaborative Robots

Lionel Birglen

Received: date / Accepted: date

Abstract This paper presents the design and optimization of a self-adaptive, a.k.a. underactuated, finger targeted to be used with collaborative robots. Typical robots, whether collaborative or not, mostly rely on standard translational grippers for pick-and-place operations. These grippers are constituted from an actuated motion platform on which a set of jaws is rigidly attached. These jaws are often designed to secure a precise and limited range of objects through the application of pinching forces. In this paper, the design of a self-adaptive robotic finger is presented which can be attached to these typical translational gripper to replace the common monolithic jaws and provide the gripper with shape-adaptation capabilities without any control or sensors. A new design is introduced here and specially optimized for collaborative robots. The kinetostatic analysis of this new design is first discussed and then followed by the optimization of relevant geometric parameters taking into account the specificities of collaborative robots. Finally, a practical prototype attached to a very common collaborative robot is demonstrated. While the resulting finger design could be attached to any translational gripper, specifically targeting collaborative robots as an application allows for more liberty in the choice of certain design parameters and more constraints for others.

Keywords grasping · robotic hand · collaborative robots · underactuation

Lionel Birglen
Polytechnique Montreal
Montreal, QC, H3C 3A7, Canada
Email: lionel.birglen@polymtl.ca
Tel.: +1-514-340-4711
Fax: +1-514-340-5867
E-mail: lionel.birglen@polymtl.ca

1 Introduction

Self-adaptive or underactuated hands and fingers as described in [8] have been successfully introduced throughout the robotics community, both in academia and the industry, as a middle ground solution between classical industrial grippers and complex anthropomorphic robotic hands. While keeping the control simplicity of the former, underactuated grasping allows for the shape adaptation of the latter to the complex surfaces of common objects. The application of underactuation to robotic hands relies on two complementary principles: first, a transmission mechanism is used to distribute a single actuation force or torque to the many joints of the (driven) finger; second, a set of passive elements are used to statically constrain the resulting mechanical device. The transmission mechanism can take the form of a linkage and, typically, preloaded springs maintaining the phalanges aligned when no contact has yet occurred serve as the passive elements. Notice however that the transmission mechanism can also be implemented using cables and pulleys as shown in maybe the earliest prototype of underactuated gripper, the Soft Gripper [15]. The number of phalanges of this latter device, namely ten, is rather peculiar and anthropomorphically inspired designs with three phalanges are much more common, e.g. [11, 12, 21, 22]. When compared with fully actuated designs, underactuated fingers have an attractive simplicity since they typically require only one actuator, and do not rely on sensors or complex control scheme.

During the last decade, underactuated hands and fingers have migrated from university research centers to the industry and several companies have emerged to commercialize these end-effectors, such as Barrett Tech-

nology, Robotiq, Lacquey, and RightHand Robotics for the most well-known. Yet, the manufacturing and packaging industry still mostly relies on parallel grippers for their operations and is reluctant to replace them since they have been using these for decades sometimes. Indeed, the end-of-arm-tooling of choice for mechanical robotic manipulation seems to remain the classic parallel grippers (barring suction cups.) However, there is a solution to take advantage of the benefits of underactuated grasping while preserving the familiarity and know-how of the industry. This solution consists in using self-adaptive robotic fingers that can be attached to the usual industrial grippers in replacement of the monolithic jaws and thereby transform the tool into a fully functional underactuated hand at a very low cost. This principle was embodied for the first time maybe in the FinGripper by Festo GmbH which was constituted by a compliant structure driven by the motion at its base. A more recent device based on a similar idea was presented in [10] where translational rods connected by pneumatic struts produced an effect similar to a spring-loaded bed of pins. Recently, a variation of a previously developed finger design was proposed in [2] that is similarly intended to be attached to a three-jaw concentric industrial gripper, although in this case another supplementary actuator is still required to initiate the enveloping motion of the finger.

In an earlier version of this work, the author himself presented in [4] the PaCoMe finger: a fully passive three-phalanx self-adaptive mechanical finger capable of producing stable power (enveloping) and precision (pinch) grasps. That finger ressembles the FinGripper but uses rigid links. A prototype of this design, attached to an off-the-shelf translational pneumatic gripper, was successfully demonstrated in that reference. In the present paper, which is an extended version of the previous work, a refined and simplified version of this latter design is introduced and shown to be a valid alternative both theoretically and based on experimental results. This novel design is also specifically dedicated to be used with collaborative robots (cobots) or more precisely, to be attached to their translational grippers and takes advantage of the intrinsic safety of these cobots to alleviate some design requirements. Finally, a recent paper [14] also showed an interesting adaptive finger relying on the translational gripper of the Baxter cobot to provide actuation but that design required physical modifications of the gripper, conversely to the solution proposed here.

2 Grippers for Collaborative Robots

Cobots, are designed for human-robot collaboration, i.e. working in close proximity to humans. Amongst the most well-known and successful cobots one can find: the Universal Robots UR series, Fanuc's CR-35iA, Kuka LWR series, Rethink's Baxter and Sawyer, ABB's Yumi, and Gomtec's Roberta series (note: Gomtec was recently purchased by ABB.) It should be noted that the latter three manufacturers all provide standard translational grippers with their collaborative robots.

As the interface with the physical world, the end-effector of a robot is almost invariably indispensable. It can take many shape and form depending on the process that is automated but manipulation through grasping remains a preferred application due to its often repetitive nature and low skill requirement [5,23]. Many manufacturers offer a wide range of solution for this task amongst which: Schunk, Festo, PhD, Gimatic, Zimmer, etc. Recently, many of the latter companies as well as startups began to release on the market grippers specially dedicated to cobots such as: the Schunk Co-act, Dahl DAG-M, Gimatic KIT-UR-G/V, Weiss CRG 30, ON Robot RG series, Zimmer GEH6060IL series, and the Robotiq 2- and 3-finger hands. This recent surge of new products highlights the need for grasping solutions adapted to cobots. A common feature of all these previous grippers is a more or less seamless integration with cobotic systems. In particular, since most cobots make electrical lines available at their output flange, all the aforementioned cobot grippers rely on electricity as a power source while pneumatic seems far more popular with other non collaborative robots.

The design of these cobot grippers, conversely to the cobots themselves, has no available standard at the moment. However, since the tool is expected to be in close proximity with a human operator, most manufacturers follow the general guidelines provided in [16] namely limiting output power, avoid sharp edges, and eliminate pinch points. Limiting output power in the case of a cobot gripper typically takes the form of a capped force output since velocity is commonly smaller with electric gripper compared to pneumatic ones but forces can still be large. For the cobot itself, velocity is limited and completed by collision/force sensing. This intrinsic limit on velocity to ensure safety also make cobots more suited for tasks where high throughputs are not required, e.g. batch manipulation of small series of parts with variable sizes such as bin picking or packing. Hence, cobots are an attractive target for flexible graspers. Additionally, the force sensing available

for the cobot can also be used recognize collisions at the end-effector level as for example with the Kuka LBR in which:

> "torque sensors are built into the joint mechanism on the output side of the gearing. This means we're able to sense what's really going on at the joint level and end effector level"

(Michael Gerstenberger quoted from [1]). Improvements in sensing techniques has no doubt continued since these sentences were first stated in 2013.

In the author's previous such as [3,8], all the proposed designs of fingers and grippers were actuated by motor moving one or several joints of the fingers. The actuation torques of these motors were distributed to all the output joints of the fingers. In the more recent work [4] mentioned before, the closing motion of the finger is provided by an external prime mover, typically a traditional robotic gripper, and the finger itself is completely passive except for internal compliance. While the finger has no actuators, its contact forces can still be computed as shown in [4] and related to the input closing force of the gripper onto which the finger is attached. However, this finger was not designed for use with cobots but for applications requiring larger forces (an industrial translational gripper was used), resistance to collision, and the design had a major safety issue with pinch points. The latter problem being that a human is perfectly able to fit several of his/her fingers in an area that collapses during the closing motion of the gripper as shown in Fig. 1. The force of the industrial gripper used is sufficient to cause major damage or at least severe pain. In this paper, a new version of this passive finger is designed taking into account all the specific aspects to cobots to ensure safety but also performance.

In summary of these introductory remarks, designing a flexible grasping solution for collaborative robots is desirable due to their match with the task of manipulating various parts in small series. To this aim, using standard translational grippers as a input platform for shape adaptive fingers is an attractive solution as it allows for a smoother transition to the industry and makes use of existing hardware. When designing such adaptive fingers for cobots, three points must be taking into account:

1. contact forces must be limited,
2. sharp edges must be eliminated,
3. pinch points must be avoided.

Collision with the environment while obviously important and very damaging with traditional robots is less of an issue with cobots since they are designed to detect and react safely to these collisions. Of course, this is not an absolute rule and even a cobot has a serious potential for injury if manipulating hazardous parts (e.g. sharp blades) but a collision with the fingers is expected to be mitigated by the controller of the cobot, not necessarily the fingers themselves.

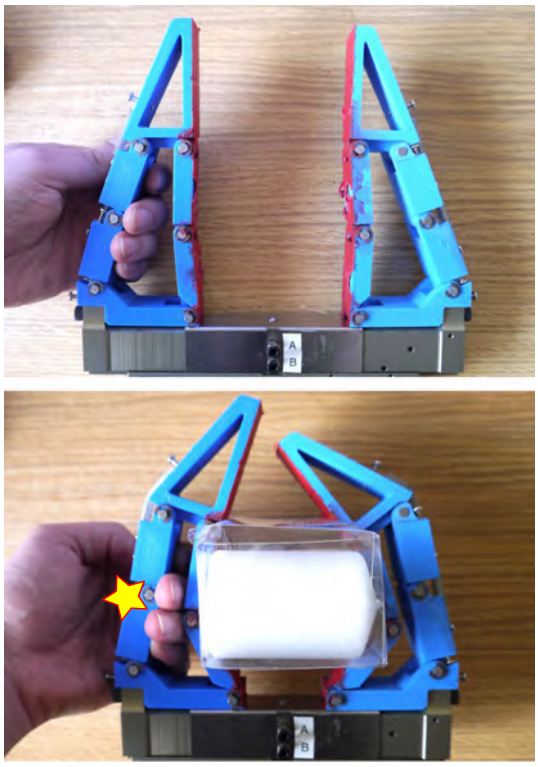

Fig. 1 Example of possible pinch points inside the PaCoMe finger. The space between the phalanges and the back of the finger is large enough for a human to fit several of his/her digits (top) into a collapsing area during the grasp (bottom). In the bottom picture, both the ring and middle fingers of the author were compressed.

3 Kinetostatic Analysis

3.1 Degrees of Freedom (DOF)

The design of self-adaptive finger previously presented in [4] and illustrated in Fig. 1 was based on a sixbar linkage with revolute joints. Four consecutive links of this mechanism were chosen as the ground and phalanges of the finger. The remaining two links constituted the transmission linkage distributing the passive element torques (from springs) to the phalanges. The three revolute joints of these two links were indeed required in the transmission linkage to avoid constraining the DOF

of the finger and ensure maximal shape-adaptivity to the object seized. However, as will be shown in this paper having a transmission linkage providing full mobility to the phalanges is arguably not critical to ensure a successful grasp as evidenced by experimental results, see Section 5. A simplified design with only two revolute joints in the transmission linkage is thus proposed here. This simplified design is illustrated in Fig. 2 actuated by a translational motion and wrapping around a part with an arbitrary shape. The kinetostatic parameters associated with the linkage are shown in Fig 3. The translational gripper on which the finger is attached is modeled by the prismatic joint at the base of the mechanism. When this joint is driven, a contact between the proximal or intermediate phalanges and the object that is to be seized creates a movement in the phalanx joints $O_1^F, \ldots, O_3^F$. These phalanges are initially constrained in the fully upright position by the springs in O_1^T and O_2^T, respectively providing a torque $\mathbf{t}_1 = t_1\mathbf{z}$ and $\mathbf{t}_2 = t_2\mathbf{z}$. The finger then deforms to accommodate the shape of the object while these passive torques generate a compliant enveloping grasp.

A set of mechanical limits is also added in the linkage to prevent this compliance from triggering when contact is established with the distal phalanx, more about this in Section 4.2. It should be noted that while the finger has three phalanges, the whole mechanism (finger+transmission linkage) constitutes a fivebar linkage and thus, has only two DOF. This basic statement implies that:

1. there is a coupling between the phalanx motions,
2. only two contacts are required to statically constrain the finger.

Both of these properties yield important consequences on the kinetostatic analysis of the finger and its performance in terms of forces and workspace, as will be shown.

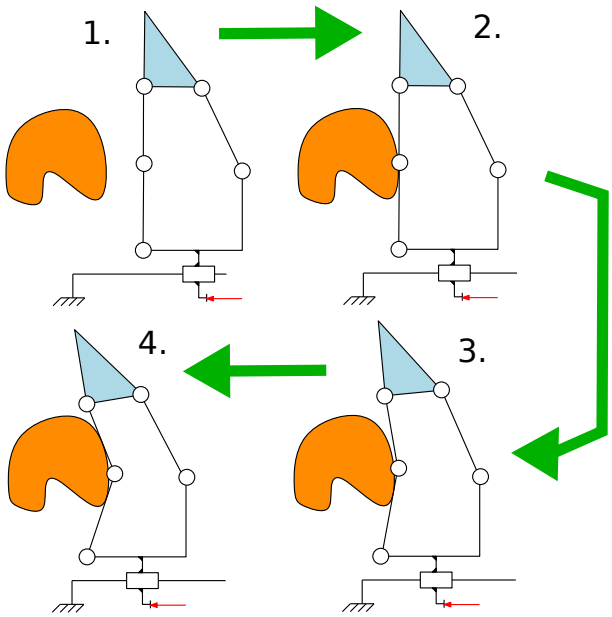

Fig. 2 Closing sequence of the proposed finger around an arbitrarily shaped object illustrating the shape adaptation, the reading order is indicated by the large green arrows and numbers

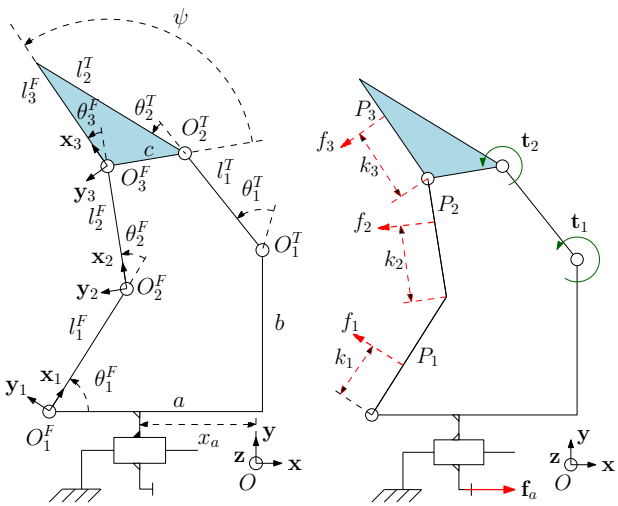

(a) Geometry (b) Force/Torque

Fig. 3 Parameters of the novel simplified mechanism: joints O_1^F to O_3^F define the phalanges, joints O_1^T/O_2^T the transmission linkage, f_a and the translation stand for the robot gripper. Contacts can occur at points P_1 to P_3 and springs create torques $\mathbf{t}_1$ and $\mathbf{t}_2$

3.2 Force Analysis

In order to establish the forces that this new design can apply onto objects, a kinetostatic analysis is proposed here following the same methodology and notations as these used in [4] which will also allow for a comparison with the latter reference. It is well-known that adaptive fingers cannot always generate positive contact forces at all phalanges. If one contact force becomes negative, the finger will reconfigure itself on the object's surface until it either reaches a stable configuration or loses contact with the object. While the former phenomenon is far more common than the latter, degeneration of the contact configuration due to negative contact forces has been shown to be very possible, see [7] for example. To establish these contact forces, assuming that dynamic forces are negligible, the virtual work principle can be used and yields:

$$\delta W = \mathbf{f}_a^T \boldsymbol{\delta}\mathbf{x}_a + \mathbf{f}_i^T \boldsymbol{\delta}\mathbf{y}^i + \mathbf{t}^T \boldsymbol{\delta}\boldsymbol{\theta}_T = 0 \quad (1)$$

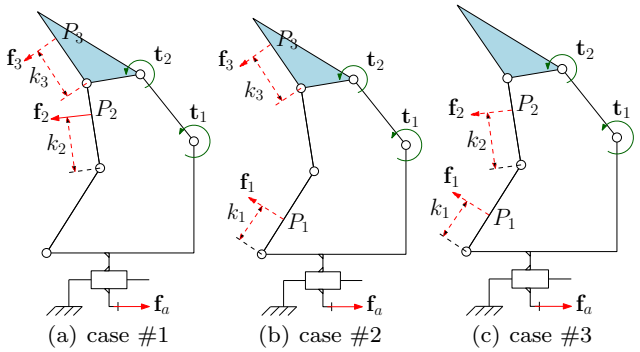

Fig. 4 Contact scenarios

where $\mathbf{f}_a = f_a\mathbf{x}$ is the force associated with the actuation of the finger itself corresponding to a translation along the $\mathbf{x}$-axis. The infinitesimal motion of the actuator is then $\boldsymbol{\delta}\mathbf{x}_a = \delta x_a\mathbf{x}$. In this paper, the notation δx and $\boldsymbol{\delta}\mathbf{x}$ stands for an infinitesimal variation of, respectively, the scalar x and the vector $\mathbf{x}$. The torques due to the springs are modeled with the vector $\mathbf{t} = [t_1\ t_2]^T$ and the rotations associated with these torques, i.e. the relative joint angles in the transmission linkage, are grouped in vector $\boldsymbol{\theta}_T = [\theta_1^T\ \theta_2^T]^T$. The vector $\mathbf{f}_i$ represents the contact forces generated by the finger at the phalanges and depends on the contact scenario i. Indeed, since only two contact points are sufficient to fully constrain the finger, three cases or contact scenarios, illustrated in Fig. 4, must be studied. Case $\#i$ is defined as a situation where the contact force f_i is missing. The contact forces themselves are assumed to be normal to the surface of the phalanges, i.e. friction is neglected, and acting along a vector $\mathbf{y}_k$ with $k = 1, 2, 3$, and the vector $\boldsymbol{\delta}\mathbf{y}^i$ is defined by:

$$\boldsymbol{\delta}\mathbf{y}^i = \begin{bmatrix} \boldsymbol{\delta}\mathbf{r}_{P_j}^T\mathbf{y}_j \\ \boldsymbol{\delta}\mathbf{r}_{P_k}^T\mathbf{y}_k \end{bmatrix} \quad \text{with } (j,k) \neq i \tag{2}$$

where $\mathbf{r}_{P_m}$ is the vector from point O to the contact point P_m which is itself at a distance k_m from the base of the associated phalanx. Neglecting friction might at first be seen as a highly impractical hypothesis for a robotic finger and frictional pads are indeed covering most existing prototypes, including the one presented in Section 5. However, as shown in [6,18], friction improves the grasp stability of underactuated fingers. Furthermore, the presence or absence of (thin) frictional pads on the phalanges does not affect the overall squeezing force which is normal to the phalanges. Thus, neglecting friction is actually a conservative hypothesis and the real performance of a finger designed thusly is expected to exceed that of the model since friction is beneficial. Taking into account friction at the design stage would also require to select the properties at the contact points (a pair of materials for instance) which are dependent on the application.

By choosing the three DOF of the mechanism (two for the finger, one for the actuation) as the translation x_a and the angles where contact occur (θ_j^F and θ_k^F for contact scenario i), a Jacobian matrix $\mathbf{J}_i$ can be defined for each contact scenario as:

$$\begin{bmatrix} \delta x_a \\ \boldsymbol{\delta}\mathbf{y}^i \end{bmatrix} = \mathbf{J}_i \begin{bmatrix} \delta x_a \\ \boldsymbol{\delta}\boldsymbol{\theta}_F \end{bmatrix} \tag{3}$$

where $\boldsymbol{\theta}_F = [\theta_1^F\ \theta_2^F\ \theta_3^F]^T$. When the transmission linkage of the finger had three revolute joints, the equivalent Jacobian matrix as defined in [4] was then:

$$\mathbf{J} = \begin{bmatrix} 1 & 0 & 0 & 0 \\ -s_1 & k_1 & 0 & 0 \\ -s_{12} & l_1c_2 + k_2 & k_2 & 0 \\ -s_{123} & l_1c_{23} + l_2c_3 + k_3 & l_2c_3 + k_3 & k_3 \end{bmatrix} \tag{4}$$

where $s_{i\ldots j}$ and $c_{i\ldots j}$ are shorthand notations for respectively $\sin(\sum_{k=i}^{j}\theta_k^F)$ and $\cos(\sum_{k=i}^{j}\theta_k^F)$. However, in our case this Jacobian matrix must be adapted to our simplified finger to take into account the reduced DOF and decrease of the contact force number.

3.3 Partial Coupling

Based upon the previous definitions, the matrices $\mathbf{J}_i$ defined in Eq. (3) can actually be established for each contact scenario simply by removing the $i+1$ line of $\mathbf{J}$, i.e. the line corresponding to the missing $\boldsymbol{\delta}\mathbf{y}^i$ of the scenario. Then, one can relate:

$$\boldsymbol{\delta}\boldsymbol{\theta}_F = \begin{bmatrix} \delta\theta_1^F \\ \delta\theta_2^F \\ \delta\theta_3^F \end{bmatrix} \text{ and } \boldsymbol{\delta}\boldsymbol{\theta}_F^i = \begin{bmatrix} \delta\theta_j^F \\ \delta\theta_k^F \end{bmatrix} \text{ with } (j,k) \neq i \tag{5}$$

through a coupling matrix $\mathbf{C}_i$ defined for each contact scenario i by:

$$\begin{bmatrix} \delta x_a \\ \boldsymbol{\delta}\boldsymbol{\theta}_F \end{bmatrix} = \mathbf{C}_i \begin{bmatrix} \delta x_a \\ \boldsymbol{\delta}\boldsymbol{\theta}_F^i \end{bmatrix}. \tag{6}$$

These matrices can be expressed as:

$$\mathbf{C}_1 = \begin{bmatrix} 1 & 0 & 0 \\ 0 & X_1 & Y_1 \\ 0 & 1 & 0 \\ 0 & 0 & 1 \end{bmatrix} \mathbf{C}_2 = \begin{bmatrix} 1 & 0 & 0 \\ 0 & 1 & 0 \\ 0 & X_2 & Y_2 \\ 0 & 0 & 1 \end{bmatrix} \mathbf{C}_3 = \begin{bmatrix} 1 & 0 & 0 \\ 0 & 1 & 0 \\ 0 & 0 & 1 \\ 0 & X_3 & Y_3 \end{bmatrix} \tag{7}$$

where the coefficients X_i and Y_i are relating the motion of the phalanx joint angle where a contact is missing to the other two phalanx joint angles. It should be noted

that the coupling matrices cannot be square since they relate a redundant set of joint positions of the linkage (δx_a and $\boldsymbol{\delta\theta}_F$, i.e. four parameters in total) to a subset chosen based on the contact scenario (δx_a and $\boldsymbol{\delta\theta}_F^i$) and of the same dimension as the number of DOF of the linkage, namely three. These matrices are therefore also of rank three.

The coupling matrices can be obtained by considering the kinematics of the two fourbar linkages defined by $O_i^F O_k^F O_1^T O_2^T$ with $k \neq i$. For example, if $i = 1$ one obtains from Eqs. (6)-(7):

$$\delta\theta_1^F = X_1 \delta\theta_2^F + Y_1 \delta\theta_3^F. \tag{8}$$

A differential form can be immediately recognized with:

$$\begin{cases} X_1 = \dfrac{\delta\theta_1^F}{\delta\theta_2^F} \text{ for } \delta\theta_3^F = 0 \\ \text{and} \\ Y_1 = \dfrac{\delta\theta_1^F}{\delta\theta_3^F} \text{ for } \delta\theta_2^F = 0 \end{cases} \tag{9}$$

and thus, X_1 can be computed by considering the fourbar defined by $O_1^F O_2^F O_1^T O_2^T$ while Y_1 requires to use $O_1^F O_3^F O_1^T O_2^T$. The reader is then referred to the literature for analytic methods to obtain the velocity relationship between the angles of a fourbar linkage, e.g. in [20]. Once the X_i and Y_i coefficients of the contact scenario considered are obtained their expressions can be substituted in Eq. (7). Then, the relationships between the velocities of all the three phalanx joints ($\boldsymbol{\delta\theta}_F$) and the two where a contact happens ($\boldsymbol{\delta\theta}_F^i$) is established. It is important to emphasize again that the coupling matrices are not square and thus, cannot be inverted to yield a solution for $\boldsymbol{\delta\theta}_F$. The system of equations described by these matrices is overconstrained. This is similar in principle to a fourbar linkage where all three joints of the mechanism can be computed knowing only the input angle. Here since the main loop of the finger is a fivebar linkage, all the three phalanx joint angles $\boldsymbol{\theta}_F$ can be computed knowing the two DOF angles $\boldsymbol{\theta}_F^i$. Adding a line to this system of equations corresponding to δx_a yields Eq. (6).

Combining Eqs. (3) and (7), one then obtains:

$$\begin{bmatrix} \delta x_a \\ \boldsymbol{\delta}\mathbf{y}^i \end{bmatrix} = \mathbf{J}_i \mathbf{C}_i \begin{bmatrix} \delta x_a \\ \boldsymbol{\delta\theta}_F^i \end{bmatrix}. \tag{10}$$

The latter equation is mostly important because it allows to relate the virtual velocity at the contact points in the normal directions of these contacts ($\boldsymbol{\delta}\mathbf{y}^i$) to the rotational rates at the phalanx joints associated with these contacts ($\boldsymbol{\delta\theta}_F^i$). Conversely to matrices $\mathbf{J}_i$ and $\mathbf{C}_i$ which were not square, their product $\mathbf{J}_i\mathbf{C}_i$ in the previous equation is and thus, can be inverted as it establishes a one to one relationship.

A last matrix is required to completely characterize the grasps of the finger, namely a Transmission matrix $\mathbf{T}_i$, relating the joint angles of the transmission linkage (hence its name) to the vector in the righthand side of Eq. (10), i.e.:

$$\boldsymbol{\delta\theta}_T = \mathbf{T}_i \begin{bmatrix} \delta x_a \\ \boldsymbol{\delta\theta}_F^i \end{bmatrix}. \tag{11}$$

This matrix can be easily established from the Transmission matrix of the original design of the mechanism presented in [4] by removing the last line of the matrix as well as the i^e column. Finally, combining Eqs. (10) and (11) into Eq. (1) yields:

$$\mathbf{f} = -(\mathbf{J}_i\mathbf{C}_i)^{-T}\mathbf{T}_i^T\mathbf{t} \quad \text{with } \mathbf{f} = \begin{bmatrix} f_a \\ \mathbf{f}_i \end{bmatrix} \tag{12}$$

where $\mathbf{X}^{-T}$ is the transpose and inverse of matrix $\mathbf{X}$. Once the contact scenario is defined based on the shape and position of an object to seize, this equation allows to compute the magnitudes of the contact forces at the phalanges as well as the required force of the translational gripper necessary to maintain the mechanism in static equilibrium. This is obviously very useful to optimize the grasping performance of the finger before building a prototype.

4 Design Optimization

4.1 Force Workspace

With the results of the previous section one can optimize a design of the proposed finger. The first question to answer is to decide what needs to be optimized. There have been quite a few performance criteria proposed in the literature, most of which have been enumerated in [19], depending on which technology is used to drive the finger (cables, linkages, deformable structure, etc.) Here, the percentage of a target workspace where all the generated contact forces are positive is chosen to be used. Indeed, as mentioned earlier, some contact force magnitudes as computed from Eq. (12) might be negative. If such a situation arises in practice the phalanx for which this occurs will move away from the object, causing a sliding motion of the finger along the object generally until a mechanical limit is reached. Alternatively, with really poor designs, if no mechanical limit prevents this reconfiguration of the finger, the sliding will continue until the object is ejected from

the finger. Using naive design parameters, an example of the typical force workspace of the mechanism proposed in this paper is illustrated in Fig. 5 for contacts at mid-phalanx and unitary stiffnesses of the springs. In this example, different undesired areas are clearly visible where:

1. the design cannot be assembled (links are too short),
2. at least one contact force is negative,
3. mechanical limits would be reached.

It can be clearly seen that maximizing the area where all contact forces are positive would be desirable and also lead to increasing the reachable workspace of the finger.

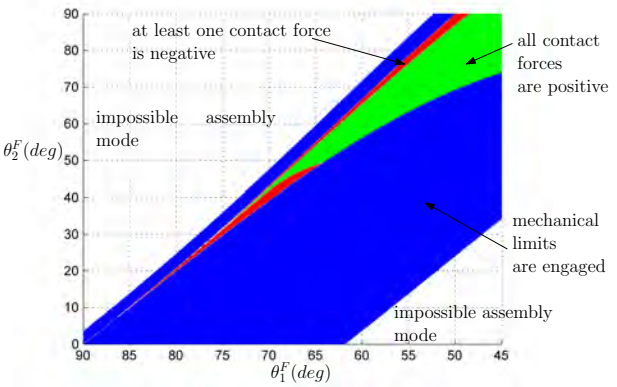

Fig. 5 Example of a typical force workspace for a finger design

4.2 Optimization Function

Mathematically, the capability of the proposed mechanism to create positive contact forces can be measured by:

$$\mu = \frac{1}{3}\sum_{i=1}^{3}\frac{\int_W \kappa(\boldsymbol{\theta}_F^i)d\boldsymbol{\theta}_F^i}{\int_W d\boldsymbol{\theta}_F^i} \tag{13}$$

where W is the workspace of the finger in terms of phalanx joint angle ranges and $\kappa(\boldsymbol{\theta}_F^i)$ is a Kronecker symbol for the positiveness of the contact forces in the contact scenario i. It is equals to one if all $f_k \geq 0$ $(k \neq i)$ or 0 otherwise. Note that μ is dimensionless and has a maximal value of 1.

The capability of an underactuated finger to generate positive contact forces over its workspace is but one optimization metric that can be used. Several other indices have been discussed, see the work [19] again. For instance, typical objects (generally cylinders) can be considered instead of the whole workspace, as in [9] for example, or the resulting stability of the grasped objects can be studied as shown by [17]. However, the actual ability to generate contact forces might be most basic requirement for a robotic finger and is a first and foremost requirement with these other indices. Furthermore, since no particular objects or applications were a priori considered, Eq. (13) appeared an acceptable choice to measure performance.

Now, the design parameters available for the optimization must be chosen. To simplify the problem, the phalanx lengths were chosen to be $l_1^F = l_2^F = 30$ mm and $l_3^F = 45$ mm. These values correspond to a 0.75 scaled down version of the prototype presented in [4] which used a significantly larger translational gripper. The rationale for this rescaling is that the prototype developed in this paper is intended to be attached to a Baxter cobot and it was desirable that the overall length of our finger would not be larger than the longest of the standard jaws provided with the electric gripper of this robot, namely 109 mm. Furthermore, by keeping the ratio of phalanx lengths identical, comparison with this previous design is fair. Then, only four parameters remain:

1. a: horizontal distance between O_1^F and O_1^T,
2. b: vertical distance between O_1^F and O_1^T,
3. c: distance between O_3^F and O_2^T,
4. ψ: solid angle defining the distal phalanx.

See Fig. 3 where all these design variables are illustrated. Of these, the angle ψ has to be set to $\pi/2$ in order for stable pinch grasps to be achievable. Indeed, by adding mechanical limits in the joints at points O_1^T and O_2^T preventing the latter to rotate clockwise, passive stable pinch grasps can be achieved without interfering with the capability of offering enveloping grasps as illustrated in Fig. 6. For this, one must make sure that any contact on the distal phalanx will create a clockwise rotation in both joints. The simplest way to do that is by making sure that a contact force there is above O_2^T, and thus $\psi \geq \pi/2$. However, if ψ is greater than $\pi/2$, any contact on the intermediate phalanx whose line of action is above O_2^T would also be opposed by the mechanical limits thereby preventing the enveloping motion of the first two phalanges. To avoid this, one is left with no choice but to set ψ at exactly $\pi/2$ as illustrated in Fig. 7. The list of set and variable geometric parameters of the optimization is presented in Table 1. The only other parameters of the finger are the two joints' stiffnesses which are reminded to be assumed identical and unitary for the optimization. Hence, all numerical values of the contact forces are proportional to these

Table 1 Geometric parameters for the optimization.

Parameter	Values/ranges
l_1^F l_2^F l_3^F	0.75 scaled version of [4] so the total length is equal to original Baxter finger
a	variable
b	variable
c	variable
ψ	set to $\pi/2$ to avoid undesirable motions, see Fig. 7

stiffnesses, see Eq. (12).

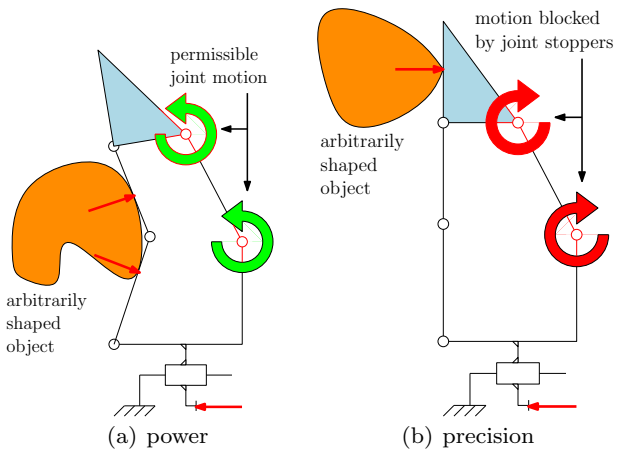

Fig. 6 Power and precision grasps achievable using mechanical limits

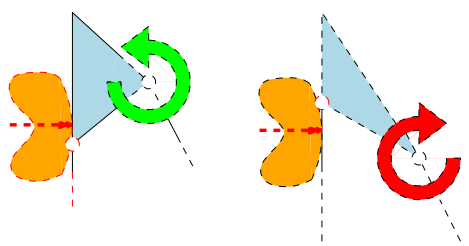

Fig. 7 Undesirable rotation of the distal phalanx (left) and blocking of the intermediate phalanx (right) when the distal phalanx solid angle is different than $\pi/2$.

4.3 Design for Collaborative Robots

In the end, three geometric parameters are available for the optimization: a, b, and c. The values and ranges of the fixed and variable parameters in the design are presented in Table 2. These ranges were chosen to avoid mechanical interferences between the links of the mechanism and with the translational gripper. It should also be noted that one attractive feature of collaborative robots is the ability to safely accommodate collisions as discussed at the end of Section 2. Therefore, while it was necessary in [4] to have the lowest joint of the transmission linkage as close as possible to the base (i.e. $b = 0$) to make the finger collision-safe, this requirement can be relaxed here since the robot is detecting collision by itself and stopping before potentially damaging forces arise. This is one of the reasons why the design proposed here is said to be targeted for cobots: collisions with the finger are not a concern and do not yield additional design constraints.

While taking advantage of the inherent safety of cobots, it should be pointed out that the finger optimized here must follow the three guidelines listed in Section 2. By using the existing gripper of a cobot and since our fingers are entirely passive with no actuators in their structure, the requirement to limit hazardous grasp forces is actually taken care of by the force limit on the gripper itself. Therefore point #1 of Section 2 does not have an impact on the geometric parameters of the fingers. Additionally, the stiffness of the springs in the transmission linkage has been shown in [8] to decrease contact forces and is also usually kept low in practical prototypes and is neglected. This will be exemplified in Section 5 where it will be shown that indeed, enveloping grasp forces produced by the fingers are of slightly lesser magnitude than the actuation force of the gripper. Therefore, if the gripper force level is safe so will the fingers'.

Point #2 can be easily solved by rounding all the edges of the mechanism at the later CAD stage. In the end, only point #3, namely pinch point avoidance, is of importance when selecting the design parameters during the optimization. Pinch points between the joints can be avoided by proper clearance selection but a major pinch point exist with the proposed design: the inside of the geometric loop defining the fingers, see Fig. 1. To mitigate this danger, the width of the inside area of the finger (the area of the inscribed polygon $O_1^F O_2^F O_3^F O_2^T O_1^T$) should be kept small enough to prevent a human to easily put his/her own finger inside the mechanism. This requirement also contrasts with the initial design presented in [4] where this property was not considered at all. Therefore, the final optimization process can be

Table 2 Range of the geometric Parameters for the optimization of the finger (all lengths are in mm).

Parameter	Values/ranges
l_1^F	30
l_2^F	30
l_3^F	45
a	[10,60]
b	[0,50]
c	[10,60]
ψ	$\pi/2$

described by:

$$\begin{aligned} &\underset{a,b,c}{\text{maximize}} \quad \mu(\boldsymbol{\theta}) \\ &\text{subject to} \quad d(\mathcal{C}_{max}) \leq w \end{aligned} \tag{14}$$

where d is the the diameter of the largest circle $\mathcal{C}_{max}$ inscribed in the polygon defined by $O_1^F O_2^F O_3^F O_2^T O_1^T$ and w is a measure representing the typical diameter of a human finger, assumed round as a first approximation. The largest area of the polygon is in the rest configuration of the finger illustrated in the upper line of Fig. 2 (positions 1. and 2.) since all joints only allow motion towards the inside of the polygon, it is therefore this configuration that must be inspected.

4.4 Results

An example of the values of the performance index μ as functions of a and b for different c is illustrated in Fig.8. The contact forces were evaluated for contacts at mid-phalanges and assuming springs of equal and unitary stiffnesses in joints O_1^T and O_2^T. The workspace of the finger was defined by:

$$W \equiv \begin{cases} \pi/4 \leq \theta_1^F \leq \pi/2, \\ 0 \leq \theta_2^F \leq \pi/2. \end{cases} \tag{15}$$

The best performance possible for a design as a function of c is illustrated in Fig. 9. Note that in the latter Fig., a minimal value of $c = 5$ mm was used to clearly show the peak around $c = 12$ mm. From these results, one can clearly see that it is beneficial to keep c small. However, values below 15 mm are difficult to design as the axes and housings of the joints at O_2^T and O_3^F tend to interfere. In practice, and again to avoid mechanical interference, a value of 15 mm for c was selected. As can clearly be seen in Fig. 8, large values of a are typically preferable for most values of c. However, in our case with $c = 15$ mm, this would lead to a very bulky design. There is therefore a trade-off to be made between performance and compactness. Taking as a measure of the latter the value of a, i.e. the width of the finger, the optimal value of b for each a as well as the Pareto front (trade-off curve) between a and μ is illustrated in Fig. 10. Selecting the value of c also simplifies the constrain of the optimization presented in Eq. (14) since now for an inscribed circle of diameter w to fit inside the finger polygon, only a and b must be inspected. Adding the compactness criterion, the optimization becomes multi-objective and can be described by:

$$\begin{aligned} &\underset{a,b}{\text{maximize}} \quad \mu(\boldsymbol{\theta}) \\ &\underset{a}{\text{minimize}} \quad a \\ &\text{subject to} \quad d(\mathcal{C}_{max}) \leq w \end{aligned} \tag{16}$$

Selecting $w = 19 + 7 = 26$ mm, the allowed design space obtained is illustrated in Fig. 11. This value of w corresponds to the sum of one digit (the unit), i.e. the average breadth of the human finger (19 mm) to the practical width of the links of the mechanism (7 mm), see Section 5. The frontier between permissible and unacceptable designs is computed numerically by searching for the largest circle that can fit the polygon of the finger. For a (presumably round) human finger to enter the internal gap of our design, a and b should be in the "unacceptable design" area of the plot. If one considers only the designs on the Pareto curve illustrated in Fig. 10, the proportion of unacceptable designs is illustrated in Fig. 12.

Dynamic simulations were also conducted using MSC ADAMS^{TM} as illustrated in Fig. 13. Notice in this figure how the design with a smaller a both leads to mechanical interference as well as a significantly smaller contact force at one phalanx. This low force is on the verge of becoming negative (vanishing) conversely to the second design (larger a) which shows much more balanced forces.

As a final choice between all solutions on the Pareto front, it was decided to keep a at 25 mm to have to safe compact design with high performance. Then, looking at Fig. 10, the best value for b was 31 mm which gives a final performance index of $\mu = 0.07$. As a comparison, the absolute best design with the parameter ranges listed in Table 2 reached a performance index of 0.11. A degradation in grasp performance was therefore accepted for the sake of an improvement in the compactness performance and safety. The final geometric parameters being amongst the permissible designs of the design space, the finger is deemed safe to use with a

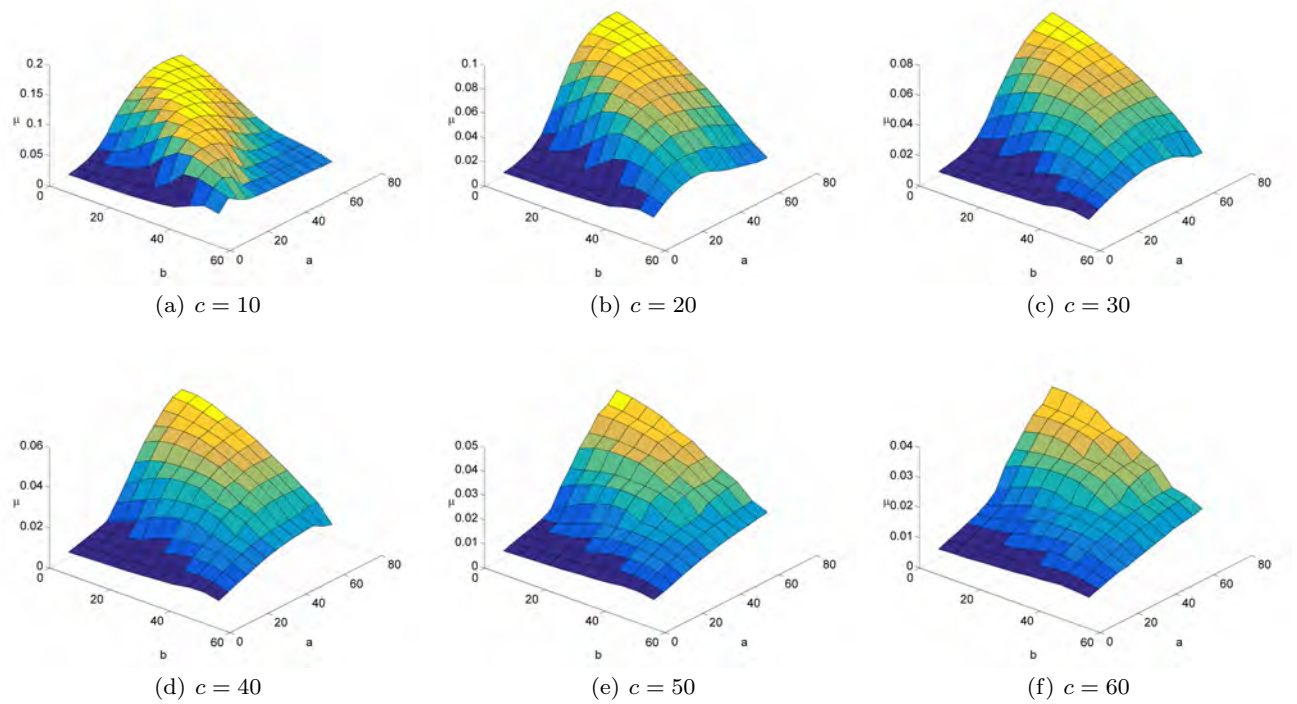

(a) $c = 10$ (b) $c = 20$ (c) $c = 30$

(d) $c = 40$ (e) $c = 50$ (f) $c = 60$

Fig. 8 Performance index as a function of a and b for different values of c (all values of a and b are in mm)

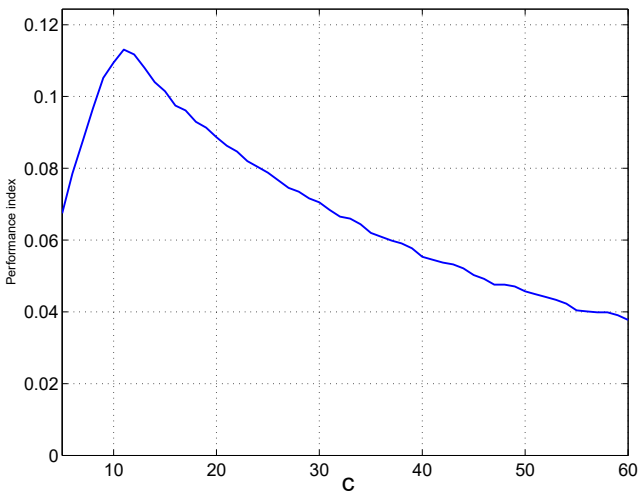

Fig. 9 Best performance index possible as a function of c (mm)

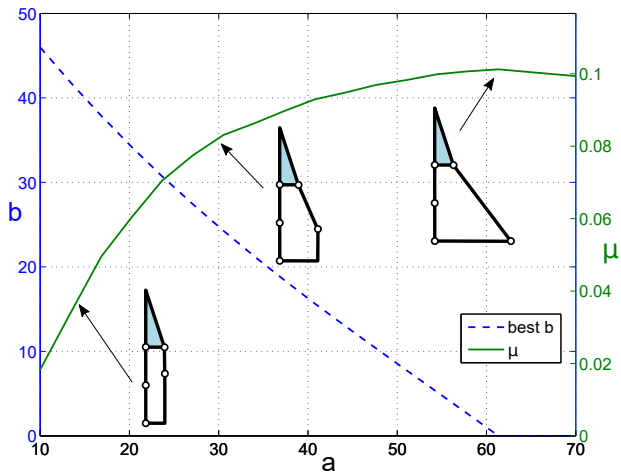

Fig. 10 Optimal values of b for each a (dashed blue) and Pareto front (μ) of the optimization, both for $c = 15$ mm. Large values of a lead to bulkier designs, the trade-off between compactness and performance is illustrated by the Pareto curve (solid green) indicating the degradation of μ with the improvement of a (lower values of a equal better compactness but lead to lower values of μ.)

cobot: the risk of a human finger to get stuck in the linkage while in operation, if not completely eliminated as w is only an average value, is relatively limited. It should also be noted that the forces developed by the Baxter electric gripper are low enough for this issue to not be a insurmountable concern, see Section 5 again for actual numbers. Indeed, this is in agreement with ISO standard of cobots [16] which also recommends using many layers of safety and not to rely on a single device or property. In our case, the mechanical layer (avoiding pinch points by limiting the fingers' gap) is completed by the actuation force limit.

Another comparison in terms of performance could be

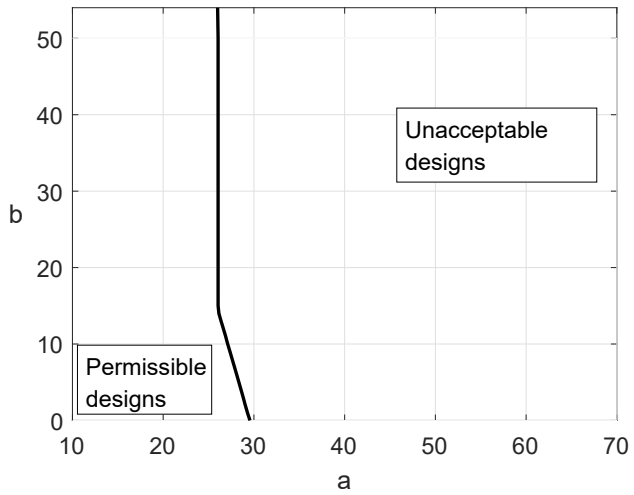

Fig. 11 Design space illustrating the optimization constraint set to avoid pinch points inside the finger, i.e. a gap between the phalanges and transmission linkage large enough for a human finger to enter)

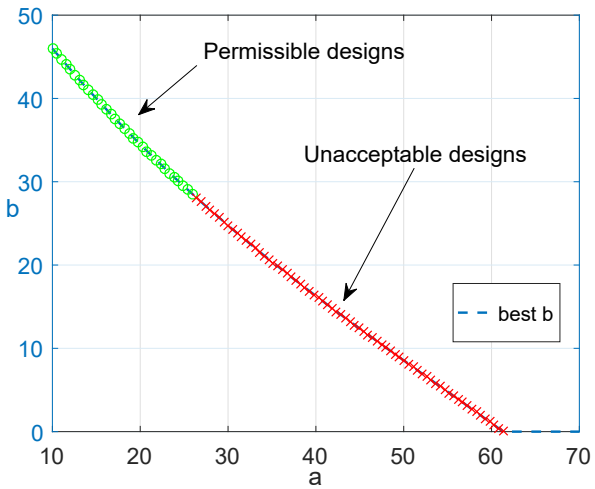

Fig. 12 Permissible values of the link lengths to prevent pinch points

made with the (not simplified) design with non-coupled phalanges presented in [4] which reached a value of 0.10 with a similarly defined performance index. Although in that case, the comparison is not entirely accurate since we are comparing between indexes computed from three two-dimensional workspaces (here) to one that is three-dimensional (non-coupled phalanges), it seems to indicate that the diminished grasp performance obtained by using the partially coupled design presented here remains limited and if compactness is not a concern, an even slightly better performance can be achieved. That is, the percentage of the finger workspace with fully positive contact forces can be approx. 10% larger with the coupled design (the performance index goes from 0.10 to 0.11). This strengthens the argument proposed by this paper that a full-mobility adaptive finger might not be required. However, if theoretical properties appear encouraging, actual physical experiments are required to ensure that the introduction of a coupling and therefore, reduced mobility for the finger is not detrimental to the capability of grasping various objects. This last point will be clearly illustrated in the next and final Section.

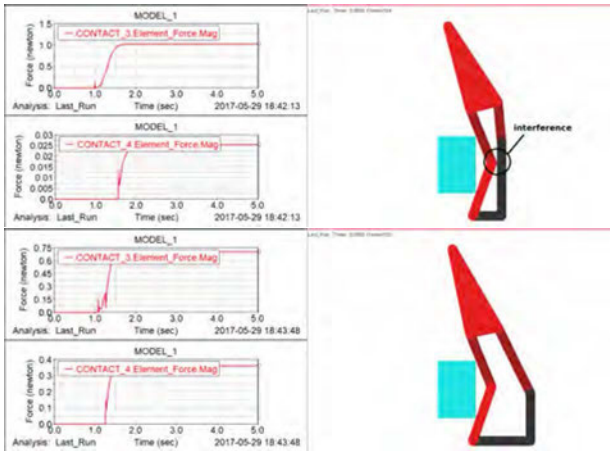

Fig. 13 Dynamic simulations of grasps with contact force measurements

5 Experiments

5.1 Design

Finally, a prototype was built based on the optimal design previously found. The adaptive fingers were built with a fused deposition modeling rapid prototyping machine in a material with properties very similar to ABS. The springs are of-the-shelf components selected for their small size and high compliance. They are made from CS70 high carbon spring steel (zinc plated) with a zero-load length of 25.4 mm and a diameter of 5.6 mm. Their measured linear stiffness was 4.3 N/mm. The inside surfaces of the fingers were covered with a thin (0.8 mm) neoprene cover with a Shore 40A durometer to provide increased adherence which is helpful to oppose the pulling of seized object in the direction perpendicular to the plane of action of the fingers (**z** axis in Fig. 3). These neoprene sheets have a typical dry static friction coefficient ranging from 1.4 to 2.2 with typical materials such as glass and steel according to the ASTM D-1894 specifications and are easy to cut which make them a popular choice for applications where increased friction is desirable such as grasping.

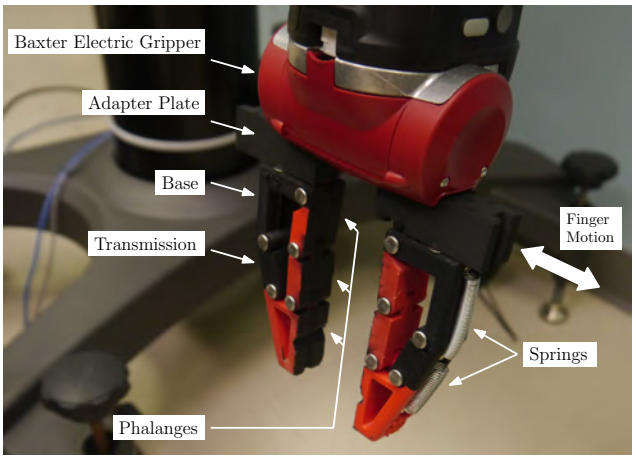

Fig. 14 Prototype of adaptive fingers mounted on the electric gripper of a Baxter robot

The actual prototype is illustrated in Fig. 14. Its installation on the Baxter robot is shown in Fig. 15. Notice that the adapter plate could actually be combined with the base of the finger in a single piece but having two different parts allows for more flexibility as the fingers can be secured in many positions onto the adapters similarly as how the original fingers of Baxter's electric gripper can also be attached in many offset positions. The fingers can then be operated by the usual software library provided by the manufacturer of the gripper without any modifications and they were found to work well for a variety of objects both in power and precision grasps. The range of motion of the fingers is dictated by the translation range of the Baxter electric gripper namely 20 mm for each finger which makes the whole hand (translational gripper + adaptive fingers) able to grasp objects in the range of 0 to 40 mm although very small objects (think of a needle) can be impractical to seize with an enveloping grasp due to clearance in the joints of the mechanism. In practice, the minimal size of the objects as projected along the translational direction to ensure a safe and secure grasp was found to be around 5 mm. As a comparison, Robotiq two- and three-finger adaptive grippers require a minimal size of 20 to 43 mm for enveloping grasps according to their specifications. Minimal object sizes do not seem to be available in the literature for other commercial grippers such as the BarrettHand or FinGripper. It should be noted that smaller objects such as the aforementioned needle could still be efficiently seized with the fingers proposed here but using a pinch grasp similarly to the way humans seize small objects.

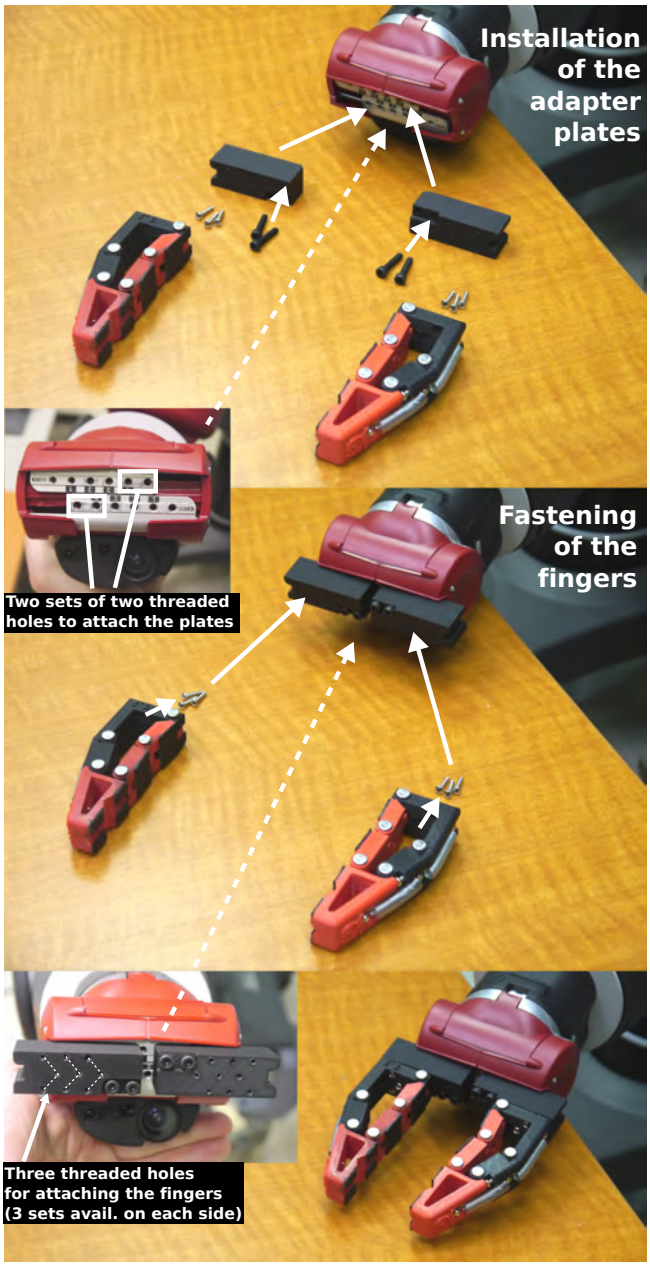

Fig. 15 Installation sequence of the fingers

5.2 Measurements and Comparisons

The adaptive fingers proposed here can be attached in several different positions on the adapter plate (see Fig. 14) so while the total motion span is always 40 mm, the grasping range can be 10 to 50 mm, or 20 to 60 mm, etc. up to 40 to 80 mm. Greater ranges could be obtained with longer adapter plate even, if required. Three pairs of half-cylindrical shells were 3D printed and embedded with 6-axis force sensors, namely either an ATI-IA NANO17 or MINI45, as illustrated in Fig. 16 to measure the grasping forces. The results are listed in

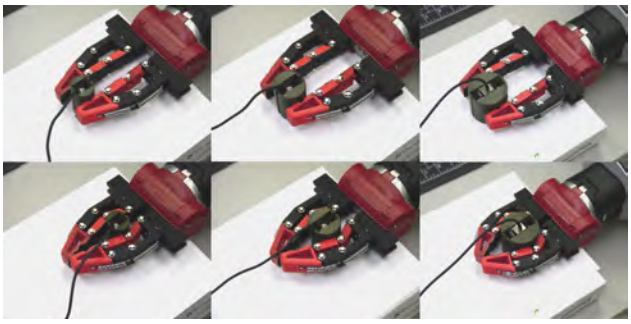

Fig. 16 Power and precision graps of cylindrical objects with force sensors

Table 3 Measured grasping forces.

Cylinder diameter (mm)	26	35	52
Sensor Model	Nano17		Mini45
Average values			
Power Grasp Force (N)	15.90	15.29	15.07
Pinch Grasp Force (N)	18.17	17.25	16.37
Standard deviations			
Power Grasp Force (N)	0.77	1.14	2.61
Pinch Grasp Force (N)	1.21	0.50	0.81

Table 3 along with the cylinder diameters. Each number in this Table corresponds to the magnitude of the squeezing force (i.e. the sum of all the individual contact forces) and is an average obtained from 10 tries (typical results are within ± 5 %.) Note that for the 52 mm cylinder, the position of the fingers was chosen for the hand to have a grasp range of 20 to 60 mm (illustrated in Fig. 16 rightmost column.)

One can see from Table 3 that the measured forces are quite similar and all between 16 to 18 N, to be compared to a range of 4 to 7.5 N reported by [14] which latter gripper has however a greater sweeping range that the one of the fingers here. Precision grasps are approximately 10-15 % stronger that power grasps for our adaptive fingers. Usually, power grasps yield stronger forces than precision grasp. However, in our case it is the opposite. The reason for this is double. First, power grasps are stronger when the fingers are actuated by a constant torque at the base since the contact forces are at a shorter distance from the actuator than for precision grasps and the product between force and distance must stay constant a shorter distance yield a larger force. However, in our case the actuation is a force so its magnitude is the same wherever contacts are established. Why power grasps are actually weaker here and the second reason for lower contact forces than with pinch grasps is that for former, part of the electric gripper force is used to flex the springs in the transmission linkage, which reduces the available output contact forces. This emphasizes the need to keep the stiffness in the springs as low as possible. Standard deviations during power grasps are also a bit higher than during pinch grasps as the fingers do not wrap around the object exactly the same way each time. The differences stay small however. Pinch forces measured with the original Baxter monolithic fingers are the same as the pinch forces measured with the fingers proposed here since during this type of grasp, the latter are essentially the same as the former, cf. Fig. 6(b). However, resistance to extraction of the object using Baxter's original fingers is much more limited since in that case only two opposing forces are available and pulling in the direction perpendicular to these two contact forces is only opposed by friction unless custom padding is added. Conversely, the fingers proposed here can envelope a wide range of objects. This envelopment leads to several contact points and thus, forces with different directions which can oppose a perturbation coming from a wider range of possible orientations.

A typical example of the force measured during a grasp and release of one sensorized cylinder is illustrated in Fig. 17. It can be seen that if the power grasp is slightly slower to get to a steady-state value due to the time required for the fingers to flex around the object, this remains marginal (from 70 ms to 98 ms.) A video demonstrating the capabilities of the hand for a set of five random objects (three were picked from the 2016 Amazon Bin Picking Challenge list, two from general household items) and showing both types of grasps can be found at: `http://youtu.be/neoeVbGLkF0` while still frames from this video are shown in Fig. 18. The video shows the Baxter robot seizing two cylinders of different diameters with a power grasp as well as one rectangular box and also pinching two objects, one of which is deformable. It illustrates how the fingers seize each object effectively. It can also be noted that in the case of the enveloping grasp of the rectangular box (video only), the proximal and intermediate phalanges rotate only slightly before reaching a stable configuration, conversely to when grasping cylinders. However, in both cases a static equilibrium is reached leading to a secure hold. Each one of these grasps was programmed offline since grasp planning is beyond the scope of this paper.

Another metric of importance for a robotic gripper is its capability to resist slippage when grasping an object. This slippage can be caused by various reasons

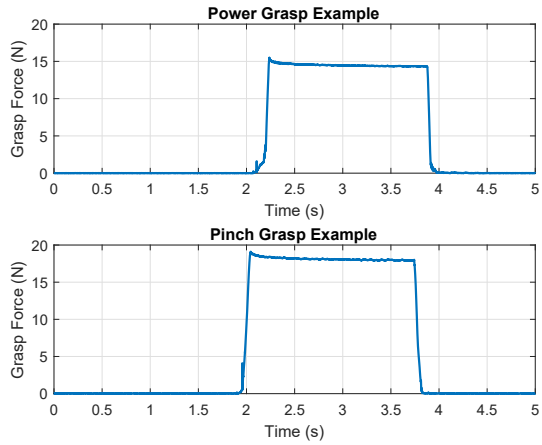

Fig. 17 Total grasp force measured by the force sensor during a grasp and release sequence (18 mm cylinder)

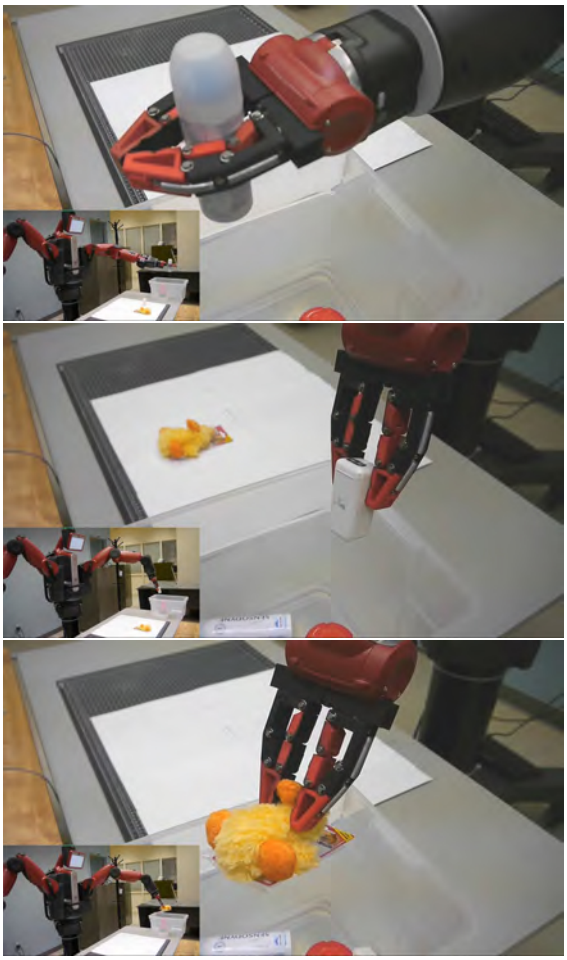

Fig. 18 Packing a box with random objects using power and precision grasps (still frames from the linked video)

but most commonly it is due to the own weight of the object when gravity acts in a direction normal to the grasp plane. Slippage is a difficult phenomenon to model and measure but a recent experimental protocol has been proposed by the American National Institute of Standards and Technology (NIST), specifically dedicated to the evaluation of slippage resistance with robotic hands [13]. In this paper, the guidelines provided by the latter reference were followed and a test bench was built. This test bench consists of a linear stage to which a uniaxial loadcell is attached on one end while the other end of this loadcell is attached to a cylinder through a cable where an elongation spring is inserted, see Fig. 19. This cylinder is then grasped by our fingers mounted again on the standard electric gripper of the Baxter robot and then, the motion platform of the linear stage is moved with a constant velocity away from the gripper in order to pull on the cylinder through the spring until slippage occurs. The pulling force is measured with the loadcell during this process and the maximal value reached is determined to be the slippage resistance of the gripper. The benefit of using the experimental protocol established by the NIST is that it provides clear guidelines as to what objects should be used (Schedule 80 PVC pipes). Indeed, slippage is obviously dependent on the pair of materials in contact and also on the magnitude of the contact forces (which varies with our fingers depending on the configuration and thus, the diameters of the pipes). An example of the results obtained when repeating five times the same experiments with both a pinch and a power is illustrated in Fig. 20. Each experiment was repeated many times and five to six typical results are shown in the plots (one experiment corresponds to one line) to illustrate deviation. The average slip resistance obtained with different diameters (these pipes have imperial sizes: nominal inside diameters are 1.5, 2.0 and 2.5 inches respectively) are listed in Table 4 and compared again to the original fingers provided with the Baxter electric gripper. The latter fingers where used with their rubber pads to increase friction and provide a fair comparison with our own design. However, it should be noted that the exact material of the pads provided by Rethink Robotics with their electric grippers is not known and appears to be different from neoprene so the comparison should be taken with a grain of salt. As can be seen from the previous table, the average slip resistances are however similar in most cases and close to the grasp force of the gripper. One can also notice from the data that the slip resistance of both our finger and the original ones from Rethink appear to be a bit weaker for smaller size objects, i.e. at the end of the electric gripper travel stroke. This trend only appears with pinch grasps and it is conjectured to be related to the shorter stroke required to fully close in power grasps relatively to pinching.

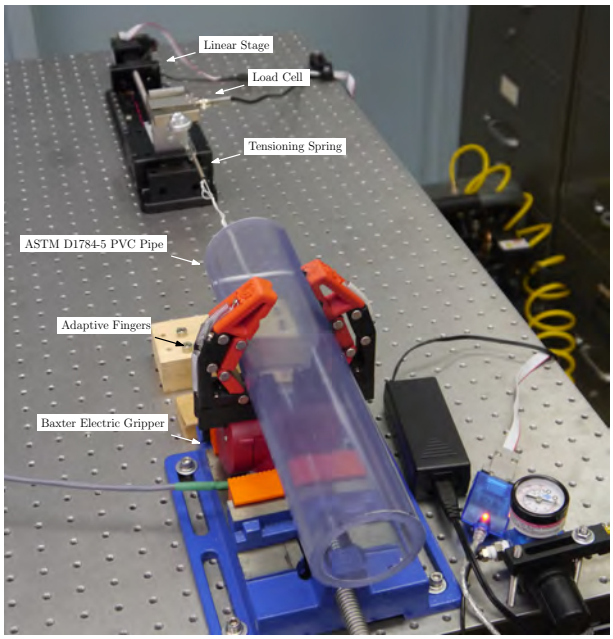

Fig. 19 Experimental setup to measure the slippage resistance (60 mm pipe shown)

Table 4 Measured slippage resistance.

Cylinder diameter (mm)	48	60	73
Average values			
Pinch Grasp (N)	16.5	19.6	21.9
Power Grasp (N)	25.5	22.2	20.0
Baxter Original Finger (N)	17.8	20.6	24.5
Standard deviations			
Pinch Grasp (N)	0.60	2.50	1.56
Power Grasp (N)	3.14	3.40	4.55
Baxter Original Finger (N)	3.89	1.42	3.48

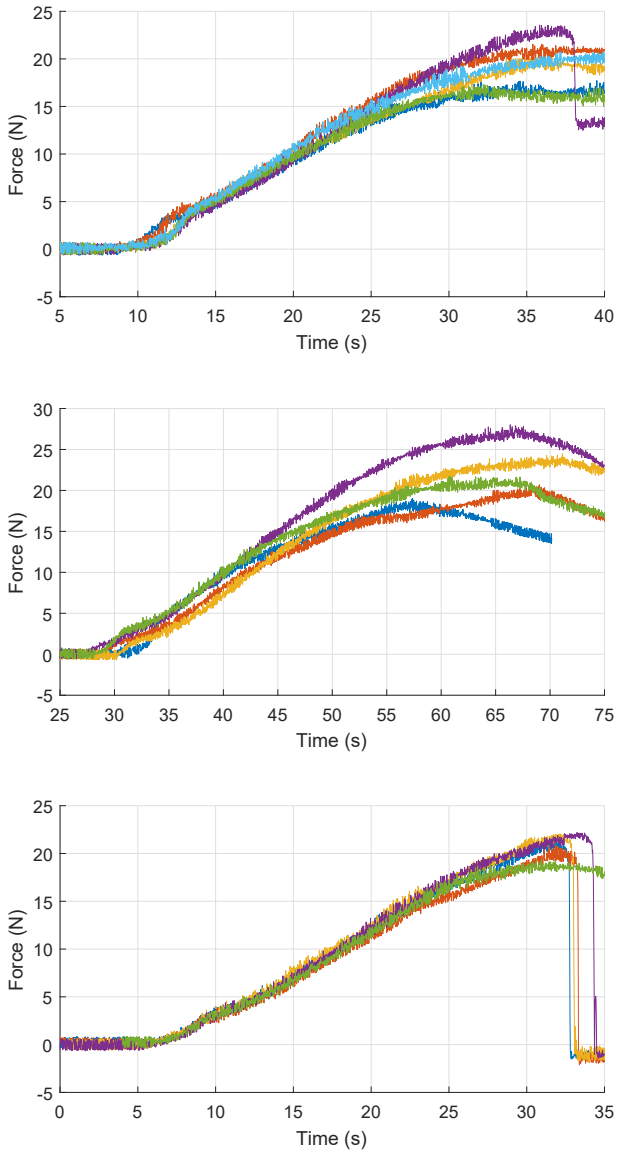

Fig. 20 Force profiles when pulling on the 60 mm cylinder during pinch (top) and power (middle) grasps. Comparison with one of the Baxter original finger (bottom). Each line of the plots corresponds to a separate experiment.

6 Conclusions

This paper presented a novel type of adaptive mechanical fingers that can be attached to the standard translational gripper of collaborative robots and transform this gripper into a fully functional underactuated hand. This design shows a simplified design compared to the geometry of previous prototypes aiming at full mobility but, as illustrated here both from theoretical and practical results, its performances appear to be at least comparable. The kinetostatic analysis of this novel design was presented and led to the introduction of coupling matrices describing specific contact scenarios. Subsequently, the generated contact forces of this mechanism were optimized and a final design was obtained by combining a performance index pertaining to these forces and the requirement for compactness. While the design discussed in this paper can be used with any translational gripper, optimizing this finger for a cobot allowed to disregard design constraints on the location of point O_1^T conversely to the previous full mobility finger. This new finger could be used with other systems than cobots but in that case, collisions with the exterior of the fingers are not necessarily safe. Finally A prototype was built and experimented with. It was shown to be able to successfully grasp and securely hold during manipulation a wide range of objects. The important lesson learned here was that simplifying the linkage appears

to be a reasonable trade-off as evidenced by the results obtained and, in particular, the practical experiments.

Acknowledgements The help of Dmitri Fedorov for the programming of the Baxter robot used for demonstration as well as Xiaowei Shan and Timothy Scott for the slippage resistance apparatus is gratefully acknowledged. The support from the Natural Sciences and Engineering Research Council (grant RGPIN327005) is also noted.

References

1. Anandan, T.M.: The End of Separation: Man and Robot as Collaborative Coworkers on the Factory Floor. Robotics Industry Insights, posted online 06/06/2013.
2. Backus, S.B., Dollar, A.M.: An Adaptive Three-Fingered Prismatic Gripper With Passive Rotational Joints. IEEE Robotics and Automation Letters **1**(2), 668–675 (2016). DOI 10.1109/LRA.2016.2516506
3. Birglen, L.: The Synthesis of Linkage-Driven Self-Adaptive Fingers. ASME Journal of Mechanisms and Robotics, **1**(2) (2009) DOI 10.1115/1.3046139
4. Birglen, L.: Enhancing versatility and safety of industrial grippers with adaptive robotic fingers. In: 2015 IEEE/RSJ International Conference on Intelligent Robots and Systems (IROS), pp. 2911–2916 (2015). DOI 10.1109/IROS.2015.7353778
5. Birglen, L., Schlicht, T.: A statistical review of industrial robotic grippers. Robotics and Computer-Integrated Manufacturing **49**, pp. 88 - 97 (2018). DOI 10.1016/j.rcim.2017.05.007
6. Birglen, L., Gosselin, C.: Grasp-state plane analysis of two-phalanx underactuated fingers. Mechanism and Machine Theory **41**(7), 807–822 (2006)
7. Birglen, L., Gosselin, C.: Optimally unstable underactuated gripper: Synthesis and applications. In: 2006 ASME International Design Engineering Technical Conferences. Philadephia, PA, USA (2006)
8. Birglen, L., Laliberté, T., Gosselin, C.: Underactuated Robotic Hands. Springer, New-York (2008)
9. Boucher, J.M., Birglen, L.: Performance augmentation of underactuated fingers' grasps using multiple drive actuation. Journal of Mechanisms and Robotics **9**(4), 041,003 (2017)
10. Carpenter, R., Hatton, R., Balasubramanian, R.: Comparison of Contact Capabilities for Underactuated Parallel Jaw Grippers for Use on Industrial Robots. In: 2014 ASME International Design Engineering Technical Conferences. Buffalo, NY, USA (2014)
11. Catalano, M., Grioli, G., Farnioli, E., Serio, A., Piazza, C., Bicchi, A.: Adaptive synergies for the design and control of the Pisa/IIT SoftHand. The International Journal of Robotics Research **33**(5), 768–782 (2014). DOI 10.1177/0278364913518998. URL `http://dx.doi.org/10.1177/0278364913518998`
12. Dollar, A.M., Howe, R.D.: A robust compliant grasper via shape deposition manufacturing. IEEE/ASME Transactions on Mechatronics **11**(2), 154–161 (2006). DOI 10.1109/TMECH.2006.871090
13. Falco, J., Van Wyk, L., Liu, S., Carpin, S.: Grasping the Performance: Facilitating Replicable Performance Measures via Benchmarking and Standardized Methodologies. IEEE Robotics & Automation Magazine, **22**(4), 125–136 (2015) DOI 10.1109/MRA.2015.2460891
14. Franchi, G., ten Pas, A., Platt, R., Panzieri, S.: The Baxter Easyhand: A robot hand that costs $150 US in parts. In: Intelligent Robots and Systems (IROS), 2015 IEEE/RSJ International Conference on, pp. 2917–2922 (2015). DOI 10.1109/IROS.2015.7353779
15. Hirose, S., Umetani, Y.: The development of soft gripper for the versatile robot hand. Mechanism and Machine Theory **13**, 351–358 (1978)
16. Robots and robotic devices – Collaborative robots. Standard ISO/TS 15066:2016, International Organization for Standardization, Geneva, CH (2016)
17. Kragten, G.A., Baril, M., Gosselin, C., Herder, J.L.: Stable precision grasps by underactuated grippers. IEEE Transactions on Robotics **27**(6), 1056–1066 (2011). DOI 10.1109/TRO.2011.2163432
18. Kragten, G.A., Bosch, H.A., van Dam, T., Slobbe, J.A., Herder, J.L.: On the effect of contact friction and contact compliance on the grasp performance of underactuated hands. In: ASME 2009 International Design Engineering Technical Conferences and Computers and Information in Engineering Conference, pp. 871–878. American Society of Mechanical Engineers (2009)
19. Kragten, G.A., Herder, J.L.: The ability of underactuated hands to grasp and hold objects. Mechanism and Machine Theory **45**(3), 408 – 425 (2010)
20. McCarthy, J.M.: Geometric Design of Linkages. Springer-Verlag (2000)
21. Ozawa, R., Hashirii, K., Kobayashi, H.: Design and control of underactuated tendon-driven mechanisms. In: Robotics and Automation, 2009. ICRA '09. IEEE International Conference on, pp. 1522–1527 (2009). DOI 10.1109/ROBOT.2009.5152222
22. Palli, G., Scarcia, U., Melchiorri, C., Vassura, G.: Development of robotic hands: The UB hand evolution. In: 2012 IEEE/RSJ International Conference on Intelligent Robots and Systems, pp. 5456–5457 (2012). DOI 10.1109/IROS.2012.6386303
23. Wolf, A. and Steinmann, R. and Schunk, H.: Grippers in Motion: The Fascination of Automated Handling Tasks. Springer Berlin Heidelberg (2005)